EurJIC European Journal of Inorganic Chemistry

FULL PAPER

DOI: 10.1002/ejic.201101075

K_β Detected High-Resolution XANES of Fe^{II} and Fe^{III} Models of the 2-His-1-Carboxylate Motif: Analysis of the Carboxylate Binding Mode

Ana Mijovilovich,*[a] Hisashi Hayashi,[b] Naomi Kawamura,[c] Hitoshi Osawa,[c] Pieter C. A. Bruijnincx,[a] Robertus J. M. Klein Gebbink,[d] Frank M. F. de Groot,[a] and Bert M. Weckhuysen*[a]

Keywords: Carboxylate ligands / X-ray absorption spectroscopy / Enzyme models / Amino acids / Coordination modes / Structure elucidation

Proteins sharing the same "2-His-1-carboxylate" structural motif have little amino acid sequence similarity and are able to perform many different reactions. Many factors have been cited to explain their different specificity and turnover rates, like protein environment, coordinated ligand geometry, electronic structure of the active site, etc. In this paper, we present a combined approach applying high-resolution XANES spectroscopy and theory simulations to different model complexes that mimic the binding modes of the amino acids to the metal site. Experiments were performed on three compounds showing three metal sites: ferrous hexacoordinate, ferric pentacoordinate and ferrous pentacoordinate. The first two compounds bear an *N*,*N*,*O*-tridentate 3,3-bis(1-alkylimidazol-2-yl)propionate ligand that features a monodentate carboxylate group. These complexes mimic the activity of extradiol dioxygenases but also exhibit intradiol cleavage activity. The third compound features a bidentate terphenylcarboxylate ligand and a sterically hindered bidentate *N*,*N*-donor, thus providing a good structural mimic of the ternary enzyme-tetrahydrobiopterin-substrate complex in pterin-dependent phenylalanine hydroxylase, which also contains a bidentate carboxylate. Modeling of high-resolution XANES on well-defined model complexes of different geometry can aid in protein structure elucidation. XANES gives the oxidation state and coordination number of the metal in the non-crystallized protein at natural pH. The accuracy of the results is limited by the core-hole and experimental broadenings. We found that high-resolution XANES experiments give increased resolution at the pre-edges, but limited improvement at the main edge. These high-resolution pre-edges can be accurately simulated by using crystal field multiplet theory (CFM). We show that by combining modelling and XANES simulations with FEFF8, detailed structural and chemical information can be obtained. We found that a short O2–metal distance for the carboxylate oxygen atom not bound to the metal causes a higher white line in Fe^{II}, which is similar to the results obtained for the pterin-dependent hydroxylase, tyrosine hydroxylase (TYH). Full-potential FDMNES simulations for each sample confirm the accuracy of the main results with muffin-tin approximation (FEFF8).

Introduction

The 2-His-1-carboxylate motif consists of a facial triad of two histidine residues and one carboxylate from either glutamate or aspartate ligands coordinated to a mononuclear iron(II) metal centre. It is common to a number of protein families but rather dissimilar in its sequence and the reactions it catalyzes.[1–4] Subtle differences are observed in the binding mode of the carboxylate ligand of the triad within this superfamily of enzymes. The extradiol catechol dioxygenases, for instance, feature a monodentately bound glutamate. These enzymes catalyze the oxidative cleavage of catechols, which is an important first step in the biodegradation of aromatic compounds. Extradiol cleaving catechol dioxygenases use ferrous iron to cleave the aromatic C–C bond adjacent to the catechol oxygen atoms, while intradiol catechol dioxygenases bearing a ferric metal centre act on the C–C bond between the catechol oxygen atoms. Many hypotheses have been put forward to explain the difference in regioselectivity displayed by the two classes of enzymes.[5,6] A new family of model compounds bearing the 3,3-bis(1-alkylimidazol-2-yl)propionate ligand has emerged[7] that mimics the activity of extradiol dioxygenase, and also exhibits intradiol cleavage activity. These tridentate, tripodal mixed *N*,*N*,*O* ligands show the same first shell ligands as in the real enzyme motif, including a monodentately bound carboxylate ligand.[7] Another family of enzymes sharing the 2-His-1-carboxylate motif is the pterin-

[a] Inorganic Chemistry and Catalysis Group, Debye Institute for Nanomaterials Science, Utrecht University,
Universiteitsweg 99, 3584 CG Utrecht, The Netherlands
E-mail: ana_mijo@yahoo.com
b.m.weckhuysen@uu.nl
[b] Japan Women's University,
2-8-1 Mejirodai, Bunkyo-ku, Tokyo 112-8681, Japan
[c] JASRI-SPring8,
1-1-1 Kouto, Sayo, Hyogo 679-5198, Japan
[d] Organic Chemistry and Catalysis Group, Debye Institute for Nanomaterials Science, Utrecht University,
Universiteitsweg 99, 3584 CG Utrecht, The Netherlands
Supporting information for this article is available on the WWW under http://dx.doi.org/10.1002/ejic.201101075.

dependent hydroxylases, which requires tetrahydrobiopterin and dioxygen for the hydroxylation of an aromatic substrate and the production of important neurotransmitters. The malfunction of these enzymes causes important neurological and psychological diseases. Upon binding of the substrate and cofactor, the monodentate glutamate becomes bidentately bound to the iron in this case. Tolman, Que and co-workers were able to synthesize accurate structural models for this particular geometric environment by making use of the flexibility of a terphenylcarboxylate in combination with a sterically hindered *N* donor.[8] The availability of these two model systems now provides an excellent opportunity to interrogate the two different coordination environments by an advanced X-ray absorption spectroscopy.

Knowledge of the coordination number in dioxygenases is important for the understanding of the mechanism of O_2 binding and substrate activation. Protein crystallography might not give the proper coordination number when many water molecules are part of the site, because of different factors (extremely low pH required to crystallize the protein, radiation damage during experiment, etc). On the other hand, X-ray Absorption Near Edge Structure (XANES) edges, including the pre-edges, are very sensitive to changes in the local electronic structure caused by oxidation state, symmetry, bonding, and coordination changes.[9–12] The pre-edge, which basically originates from the Fe 1s to 3d transition can be enhanced by the admixture of Fe 4p in the 3d levels, when the symmetry is distorted from the perfect octahedral symmetry.[12]

Changes in the geometry of the metal sites have been studied with several spectroscopic methods. For example, for 2,3-dihydroxybiphenyl 1,2-dioxygenase (an extradiol dioxygenase), the geometry of the resting state was found to be square pyramidal according to circular dichroism (CD)/magnetic circular dichroism (MCD) spectroscopic data with the aid of DFT calculations, which is not favourable for dioxygen binding, while substrate binding seems to lead to a new square-pyramidal geometry with a Fe-glutamate bond consistent with a shorter Fe–O distance found by Extended X-ray Absorption Fine Structure (EXAFS) spectroscopy.[13] Also, the combination of several spectroscopic probes (ESR, UV/Vis, Raman, IR and EXAFS) allowed the proposal of suitable models for the binding of histidine to Cu in solutions at different pH.[14] In that work, depending on the pH, the binding mode of the histidine proposed evolved from monodentate (bonded from the carboxylate end) for low pH to bidentate (both the imidazole ring and the carboxylate end bound) for high pH.

XANES simulations with FEFF8[15] have proven to be a powerful tool to study the local structure at the metal site in proteins.[16–20] In the XANES region of the spectra, though the differences for different binding modes of the carboxylate are generally small because of the core-hole and experimental broadening, the simulation of the XANES has been successful in discerning the binding mode of the carboxylate for two pterin hydroxylases.[20] More detailed analyses are possible by using High Energy Resolution Fluorescence Detected (HERFD) XANES spectroscopy.[21–23]

In this work, we compare HERFD XANES spectra, including the pre-edge, with several types of XANES simulations in order to elucidate the binding modes of carboxylates and the local electronic structure of the bound oxygen species in two structural models of the 2-His-1-carboxylate motif[7,8] (see Figure 1). We analyze the bonding at the catalytic metal site from the calculated densities of states (DOS). The influence of a perfectly symmetric first shell or the lack of a water molecule and the presence of the methyl groups are analyzed. The calculations were done with real space multiple scattering theory[15] (FEFF8) for the main edge region. FDMNES,[24] calculations using the full potential, were performed to check the influence of the muffin-tin potentials in FEFF8. Crystal field multiplet[25,26] calculations were used for the pre-edge. We also discuss what kind of information can be obtained from the pre-edges and the white line (the main edge) for unfilled d-shell metals. On the basis of this discussion, a novel approach is proposed for the study of closed d-shell metals (without a pre-edge).

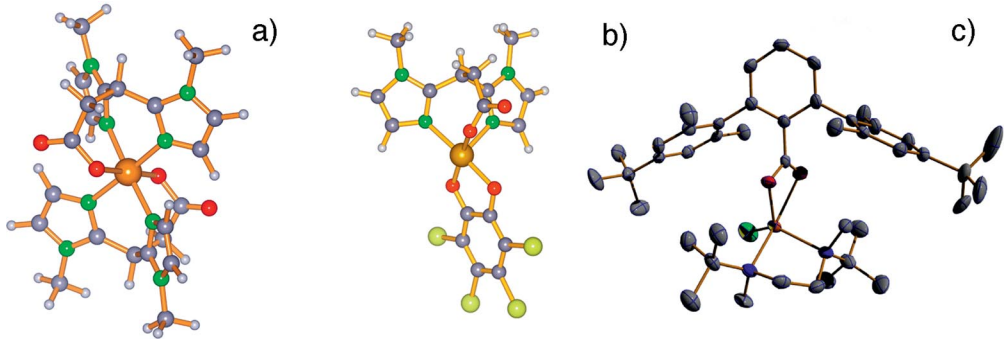

Figure 1. Computer models used for the calculations for (a) Sample **A**, [Fe^{II}(**L1**)$_2$] {**L1** = 3,3-bis(1-methylimidazol-2-yl)propionate and (b) Sample **B**, [Fe^{III}(**L1**)(tcc)] {tcc = tetrachlorocatecholate}. (c) X-ray crystal structure of Sample **C** [Fe^{II}(tBu$_2$Me$_2$eda)(BmaCO$_2$)Cl] {eda = ethylenediamine, bma = 4,4′′-di-*tert*-butyl-2,2′′,6,6′′-tetramethyl-[1,1′:3′,1′′-terphenyl]-2′-carboxylic acid}. Sample **A** and **B**: Fe: orange, C: grey (large ball), O: red, N: green, Cl: yellow, H: grey (small ball); Sample **C**: Fe: orange, C: grey, O: red, N: blue, Cl green (see Experimental Section for details).

Results

Experimental Data: Conventional and High Energy Resolution Fluorescence Detection (HERFD) XANES Spectroscopy

The conventional and the HERFD XANES spectra are shown together in Figure 2a–c for the three compounds. For all the compounds studied, the HERFD XANES spectra are very similar to the conventional ones around the absorption edge. This high similarity of the main edge (white line) is in contrast to that for the Cu complexes measured under similar experimental resolution.[27] The lack of "extra" structure in the HERFD XANES might be because of the nature of the electronic structure (no hidden structure)[23] of the present samples. On the other hand, substantial differences between the two types of XANES spectra were found in the pre-edge region: the peaks for HERFD XANES are generally sharper than those for conventional XANES. Such resolution enhancement is therefore anticipated in HERFD XANES data.

The HERFD pre-edge of Sample **A** is in good agreement with that of other 6-coordinated O_h ferrous sites in minerals (for example, siderite,[23] fayalite[22]). The highly resolved pre-edge is also similar to that of Fe_2SiO_4 shown by de Groot.[28]

The ferric five-coordinate Fe in Sample **B** gives rise to a more rounded white line. The edge position is about 3 eV above the ferrous compound (Sample **A** 7120.8 eV and Sample **B** 7124.2 eV), as expected for higher oxidation states.[9–11] The pre-edge feature is rather similar to the result for the square-pyramidal ferric iron in [Fe(salen)Cl] reported by Westre et al.[12]

The conventional XANES spectrum of the ferrous five-coordinate Fe in Sample **C**, containing one chlorine ligand, is very similar to that of the complex $[Fe(TMC)Cl]BF_4$ as shown by Westre et al.[12] in spite of their symmetry difference; the latter has a square-pyramidal structure and the former an asymmetric bidentate carboxylate bound to a metal in a distorted five-coordinate symmetry. The two peak structure in the pre-edge region is enhanced in the HERFD XANES spectrum, as for the other two samples.

Ligand Configuration Study by XANES Simulations with FEFF8

Several cases were analyzed to understand the relation between the geometry around Fe and the XANES features. The influence of the geometrical changes for the different models is more evident in the lifetime suppressed simulations. Moreover, in the suppressed lifetime simulations, the pre-edge region shows a more detailed structure.

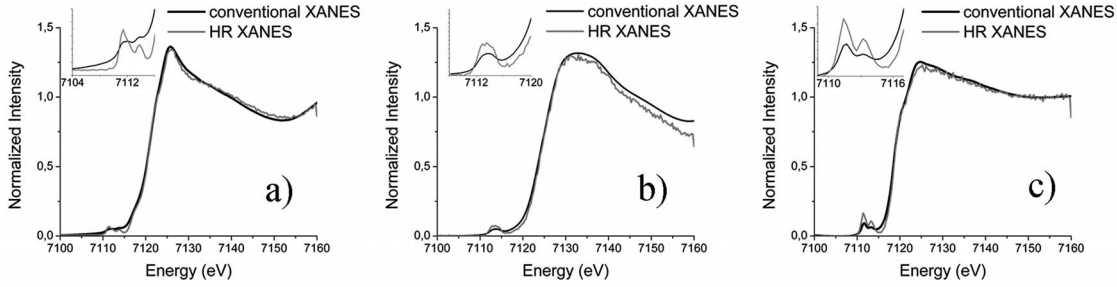

Figure 2. Conventional (black) and high-resolution (grey) XANES spectra of: (a) Sample **A** (6-coordinated Fe^{2+}), (b) Sample **B** (5-coordinated Fe^{3+}) and (c) Sample **C** (5-coordinated Fe^{2+}).

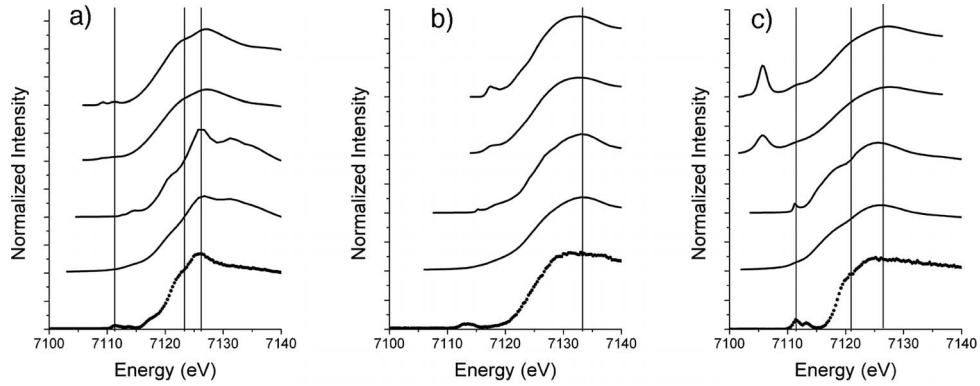

Figure 3. XANES simulation showing from bottom to top: (1) experiment; XANES simulation with FEFF8.2: (2) for core hole and experimental broadening and (3) for suppressed lifetimes; (4) XANES simulation with FDMNES for core hole and experimental broadening and (5) for suppressed lifetimes. Showing the best model of each sample: (a) Sample A (case 2 in Table 1), (b) Sample B (case 2 in Table 2) and (c) Sample C (case 1 in Table 3).

Figure 3 shows the best XANES simulations for all of the samples, and all the models tried can be found in the Supporting Information (Figure S1). The vertical lines in Figure 3 correspond to the features pointed out in the first derivatives of the high-resolution experiment (see Supporting Information Figure S2). The "goodness" of the simulation can be estimated from the derivatives and the difference spectra of the models with the experiment (see Supporting Information Figure S2, showing the best models).

For Sample **A**, the derivatives show that the shoulder at the low-energy side of the white line is better reproduced by case 5, but for case 2, the white line is centred at the edge of the experimental edge. The region after the edge in case 2 is closer to the experimental result than cases 1 and 3. The difference spectra between the models and experiment show that the edge overall shape is better reproduced in case 2.

Table 1 shows the distances of the first shell ligands to the metal for the different models simulated for Sample **A**. The influence of the *N*-methyl group on the imidazole ring of the ligand was studied in cases 1 and 2. The addition of the methyl group increases the height of the white line, which gives a spectrum rather similar to that obtained experimentally (see Figure 3a). The double feature at the white line is also present in the lifetime broadened spectrum. All the distances were fixed to the first shell distances found by EXAFS spectroscopy in molecules with ferrous six-coordinate iron.[16,20,29,30] The position of the carboxylate oxygen atom not bound to the metal was obtained from a semiempirical geometry optimization (see Experimental Section).

Table 1. First shell distances used in the XANES simulations of Sample **A** for the different models simulated. O1c and O2c are carboxylate oxygen atoms. Case 1: first shell set to one single distance to the metal, with geometry optimization of the carboxylate oxygen atom not bound to the metal, and Case 2: including the methyl groups. Case 3: geometry as in the compound with CCDC number 644244, with one water deleted, and Case 4: with methyl groups. Case 5: same as case 3 with first shell set to one single distance to the metal.

Bond/distance (Å)	Case 1/2	Case 3/4	Case 5
Fe–O1c	2.1	1.95	2.1
Fe–O2c	3.4	4.0	4.16
4Fe–N	2.1	2.12	2.1

In the cases 3 to 5, the triad was mirrored across the metal to build the six-coordinate compound. In case 3, the distances of the Fe^{III}-catechol compound were preserved. Inclusion of the methyl group in case 4 does not improve the results significantly. In case 5, all the first shell distances were set to the average distance found for low Z ligands bound to a ferrous centre in the 2-His-1-carboxylate motif.[16,20,29–31] The carboxylate group was moved in the radial direction to the metal to give a Fe–O2 distance of 4 Å. The three models show an enhancement of the second resonance on the top of the white line with respect to cases 1 and 2 and deviates from the experimental spectrum.

The best XANES simulation for Sample **B** is shown in Figure 3b, and the first shell distances of the different models tried are shown in Table 2. The derivative spectra show that the white line in case 2 is centred at the experimental edge, while the other two models show differences in the position as well in the width of the edge. The difference spectra between the models and the experiment show that case 2 is closer to the experimental profile. For case 1, the carboxylate distance is longer than in case 3, where all first shell ligands were adjusted to the usual distance for ferric six-coordinate iron found by EXAFS spectroscopy in proteins with the 2-His-1-Carboxylate motif.[16,20,29,30] The catechol is bound on the opposite face of the metal site with a distorted five-coordinate symmetry. The long Fe–O2c distance gives rise to a shoulder in the low-energy side of the white line (at 7127.5 eV). In case 2, the distorted octahedral symmetry and distances found in the crystal structure of the six-coordinate compound [Fe(L)(TCC)(H_2O)] {L = 3,3-bis(1-ethyl-4-isopropylimidazol-2-yl)propionate, TCC = tetrachlorocatechol as deposited in CCDC-644244} were preserved when deleting the water. This simulation reproduces best the experimental XANES results. In this case, the difference in the white line between the model with a lifetime and experimental broadening and the model with a suppressed lifetime is minimal.

Table 2. First shell distances used in the XANES simulations of Sample **B**. Case 1: distorted five-coordinate, long carboxylate distance, Case 2: a water deleted from the crystal structure, and Case 3: distorted five-coordinate, one first shell distance.

Bond/distance (Å)	Case 1	Case 2	Case 3
Fe–Ocat1/Fe–Ocat2	2.02/2.02	1.923/2.02	2.02
Fe–O1c	2.25	1.95	2.05
Fe–O2c	3.51	4.0	3.47
2Fe–N	2.05	2.13	2.05

The XANES simulations for Sample **C** can be seen in Figure 3c, and the coordinates of the first shell ligands in Table 3. The coordinates of the crystal structure reproduce very well the high resolution experiment. The lifetime broadened simulation reproduces well the white line, but the pre-edge feature becomes smeared out.

Table 3. First shell distances used in the XANES simulations of Sample **C**.

Bond/distance (Å)	Case 1
Fe–O1c	2.05
Fe–O2c	2.36
Fe–Cl	2.26
2Fe–N	2.22

XANES Simulations with FDMNES

The simulations with FDMNES with and without core-hole broadening are shown in Figure 3. For Sample **A** (case 2), the energy position of the shoulder at the low-energy side of the edge is accurately reproduced with FDMNES,

while FEFF gives a lower energy for the shoulder position. Sample **B** (case 2) and **C** are also well reproduced with FDMNES.

The pre-edges in the calculations with FDMNES for Sample **A** and **B** do not appear at the right energy position but show a high similarity with the experimental pre-edges. FDMNES does not include atomic multiplets, thus the splitting of the transitions cannot be reproduced (see the forthcoming section for the calculations). For Sample **C**, the energy position of the pre-edge peak is reproduced, but not well resolved.

DOS Analysis

Insight into the electronic structure of the metal site can be obtained by analyzing the densities of states (DOS) obtained with the FEFF8 XANES simulations. The transitions to the d shell in the metal could be identified from the metal d DOS[32,33] (see the arrows in the d DOS of Figure 4).

The metal p DOS is rather similar to the that of the XANES experiment for all the compounds. The metal p DOS for Sample **C** shows an extra peak before the main edge, not present in p DOS for Sample **A**.

The oxygen ligand p DOS is very similar to the DOS of the non-bonded oxygen of the carboxylate and shows little variation for the different compounds. In particular in Sample **C**, the presence of chlorine in the coordination shell of Fe does not affect the electron density of the oxygen, which is similar to the other two compounds bearing only low Z ligands (O/N) in the coordination sphere of the metal.

The analysis of the densities of states calculated with FDMNES shows that the d density of states has an overlap with the calculated pre-edges in the spectra (see Supporting Information, Figure S3). The p and d metal DOS are very similar to those obtained with FEFF. Only the p DOS for Sample **A** shows more structure at the edge position than that in the FEFF result.

Pre-Edge Calculations with Crystal Field Multiplet

The pre-edges, specially the ferrous nearly octahedral site in Sample **A**, show more detail in the high-resolution spectra than in the conventional XANES spectra. Crystal field multiplet theory has been successful in simulating this experimental data. For both the ferrous and the ferric metal centre (in Samples **A** and **B**, respectively), reduction of the crystal field parameter to 75% from the atomic values[34] was necessary (see Figure 5). However, this result is not

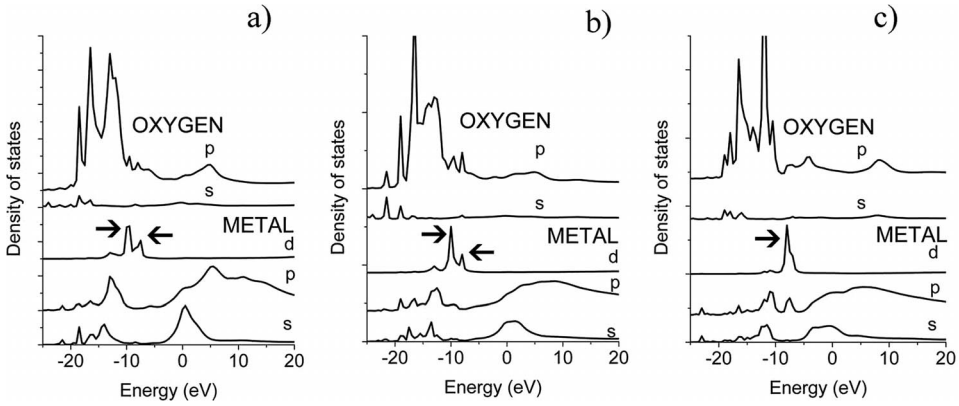

Figure 4. LDOS showing from bottom to top: s, p, and d DOS for metal, and s and p DOS for the oxygen bound to the metal for: a) Sample **A**, b) Sample **B**, and c) Sample **C**.

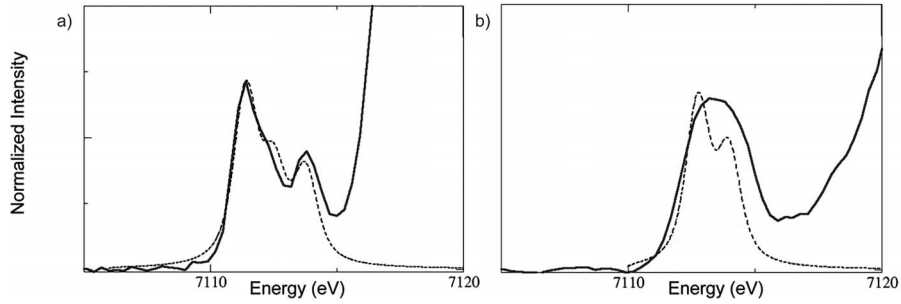

Figure 5. Pre-edge calculations by using crystal field multiplet (dashed line) compared to experimental data (solid line)for: (a) Sample **A**, (b) Sample **B**.

enough to assign a value for the crystal field in ferric high-spin compounds.[35]

Discussion

The high similarity of the main edge in the conventional and the high-resolution XANES spectra for the Fe model compounds of the different dioxygenases is in contrast to that found for the Cu complexes measured under similar experimental resolution.[27] The lack of "extra" structure in the high-resolution Fe edges in this work cannot be due to the lifetime broadening, but might be due to the nature of the electronic structure (no hidden structure).[23]

The XANES simulations indicate that small changes in the bond length of a ligand to the metal are a determinant of changes in the white line without significant change in the white line shape (case 3/4 and 5 in Sample **A**, and case 1/3 compared to case 2 in Sample **B**). Keeping the overall symmetry of the molecule intact does not introduce extra features at the edge (see Figure 3a for case 2), which gives a better agreement with the experiment. This result was also found for phenylalanine hydroxylase simulations, where the metal site from the low-resolution protein crystal structure (2 Å)[36] was "compressed" (instead of shifting the ligands towards the metal), in order to correct the first shell bonding distances according EXAFS.[16,20,29,30] It is difficult to estimate whether this result is due to a better structural model or because of constructive multiple scattering contributions that result from a more symmetric structure.

In cases 3–5, the effect of the first shell distances can be seen. In case 5, the first shell has a single distance to the metal,[16,20,29] while in cases 3 and 4, the carboxylate O1 distance is shorter. All spectra are rather similar. On the other hand, both case 2 and case 5 have a single distance for the first shell, while the orientation of the non-metal-bonded carboxylate O2 differs. In the optimized structure of Sample **A**, the carboxylate O2 oxygen atom is rotated to a shorter metal–O2 distance (cases 1–2), showing a white line in better agreement with the experimental single higher peak, while the models with a longer Fe–O2 (cases 3–5) favour the splitting of the white line. Thus, the higher white line in case 2 can then be attributed to the "carboxylate shift" between case 2 and case 5. The same result was found for TYH and PAH (phenylalanine hydroxylase),[20] where the short metal–O2 distance causes a higher white line in TYH.

A shoulder at the high-energy side of the main edge has been reported for Fe^{II} bleomycin model compounds.[37] In this work, the changes observed at the high-energy side of the main edge in cases 1–2 for Sample **A** occur at much lower energies. The decoupling of the main edge in two peaks in the FEFF8 simulation is due to the lack of full potentials, while the white line shape is accurately reproduced with FDMNES by using the finite differences method. In the FEFF8 simulations of the cases 3–5, there is a shoulder at about +15 eV, which is in agreement with the results on Fe^{II} bleomycin,[37] as caused by an imidazole-rich Fe first shell.

This sensitivity of the edge shape to structural changes is also seen in the XANES simulation by comparing the PAH and TYH carboxylate binding mode to a ferrous centre, where the rotation of the carboxylate towards a shorter metal–O2 distance in TYH accounts for the higher white line intensity in the experimental XANES spectrum.

For the five-coordinate ferric site in Sample **B**, the best agreement between XANES simulations and experiment was obtained for the distorted octahedron where a water molecule has been deleted. The round pattern in the white line resembles the features seen in ferric hydrated Fe complexes, which have been explained as double channel excitation.[38] The presence of double excitation channels and the sensitivity of the high-resolution XANES to them will be investigated in future studies.

The additional shoulder at the low-energy side of the white line of Sample **C** can be attributed to the coordination to chlorine in the model compound, which is different from the water oxygen in the enzyme (see Figure S5 in the Supporting Information, where in the FDMNES simulation the chlorine was replaced by fluor).

FEFF8 avoids the calculation of wave functions or molecular orbitals (MOs) by a formalism based on the Green function in the complex energy plane.[15] However, the relation to the MOs can be recovered by calculating the final state angular momentum projected densities of states (LDOS), from which a chemical interpretation can be made. For the compounds of this paper, the metal p DOS is rather similar to the XANES.

With regard to the pre-edge of the ferrous compounds, the FEFF8 simulation with suppressed lifetime gives a pre-edge with a single peak, instead of the two peaks observed experimentally. The transitions have been identified in the metal d DOS (see Figure 4). It has to be noted that neither FEFF8 nor FDMNES include multiplet splitting. FDMNES avoids the inaccuracies arising from the muffin-tin potentials, which gives an improved agreement with the experiment for the main edges, but lacks accuracy in the pre-edges because of the lack of multiplet treatment. In fact, the metal d DOS for Sample **C** is rather different from the DOS for samples **A** and **B**, which contain only low Z ligands in the coordination shell. On the other hand, the presence of chlorine does not affect the density of states of the oxygen atoms bound to the iron centre in the FEFF8 calculation.

In the crystal field multiplet calculations of the pre-edges, the reduction of the crystal field parameter values to 75% from the atomic values[34] indicates an important amount of covalency in the metal–ligand bond.

Conclusions

XANES spectroscopy is an important tool for the study of "noncrystalline/very dilute" systems. The high-resolution data at the pre-edge reveals the underlying structure in more detail. These high-resolution pre-edges for the *K*-edge absorption of unfilled d-shell elements show changes in the

symmetry and hybridization of the 3d levels with great sensitivity. Here, we have demonstrated that similar information can be obtained from the main edges. Similarly to the study of the pre-edges,[12] scanning over a range of different geometries for the metal centre is necessary to establish the "structure–XANES features" relationship. The XANES simulations using real space multiple scattering theory provide information with regard to the structure and coordination and the differences in the electronic structure among the different model compounds, which will be the theory basis for understanding the coordination of the amino acids to the metal in the high-resolution (main edge) XANES analysis of proteins and enzymes.

To summarize, several conclusions about the use of the high-resolution XANES spectroscopy can be drawn. The three compounds analyzed here represent three "symmetries" identified by protein crystallography for the 2-His-1-carboxylate motif:[1,39] (1) ferrous hexacoordinate (Sample **A**), (2) ferric pentacoordinate (Sample **B**) and (3) ferrous pentacoordinate metal centres (Sample **C**). The calculated XANES provide electronic-structure information (from the DOS for the metal centre, as well as information about the ligand from the ligand DOS) similar to that from the high resolution pre-edge. From the analysis of the electronic structures for the three models, aspects of the relationship between spectral features and structure emerge as well as a basis to understand the mechanistic versatility of the motif. The flexibility to bind different exogenous ligands allows the same motif to perform very different kinds of reactions in enzymes sharing low-sequence similarity. This flexibility can be explained by the "indifference" of the oxygen ligand p DOS to changes in symmetry/coordination number and exchange of O by Cl. The present work shows the subtle correlation between the orientation of the carboxylate and the absorption edge features by using a combined approach of high-resolution XANES experiments, crystal field multiplet for the pre-edges, and real space multiple scattering XANES simulations of the main edges. The effects on the XANES analysis of the orientation of the carboxylate bound to Fe^{II} is in agreement with results obtained for PAH and TYH, where the short metal–O2 bond causes a higher white line in TYH and in case 2 for Sample **A** of this paper.

Experimental Section

Sample Preparation: Samples of Fe^{III}-catecholate compound [Fe^{III}(**L1**)(tcc)] {with **L1**: 3,3-bis(1-methylimidazol-2-yl)propionate and tcc: tetrachlorocatecholate}[7] (here as Sample **B**) and the Fe^{II} six-coordinate compound [Fe^{II}(**L1**)$_2$] where the catechol was replaced by another ligand **L1** (Sample **A**) have been prepared as discussed by Bruijnincx et al.[7,40] Sample complex [Fe^{II}(tBu$_2$-Me$_2$eda)(BmaCO$_2$)Cl] with a terphenylcarboxylate ligand coordinated to Fe^{II} (Sample **C**) was prepared as discussed by Friese et al.[8] Sample **A** and **B** were placed in the holder in Ar atmosphere.

All samples have high spin[7] as seen in the $K_{\beta 1,3}$ spectrum[26] (see Figure S4 in the Supporting Information).

High-resolution XANES Spectroscopy: Experiments were performed at the beamline BL39XU at SPring-8, which consisted of a double-crystal diamond Si(111) monochromator and a cylindrically bent rhodium-coated mirror in order to focus the beam horizontally.[41] The photon flux at the sample position was estimated to be approximately 1×10^{13} photons/s, and the spot size was 0.2 mm (height) ×0.1 mm (width). Conventional XANES spectra were obtained by monitoring the intensity of total fluorescence by a Si-PIN photodiode while excitation energy is scanned. Lifetime-broadening-suppressed absorption measurements were performed by using a multicrystal, multidetector spectrometer, the details of which have been described elsewhere.[42,43] In short, the spectrometer consists of three pairs of a spherically bent Ge(620) crystal and a scintillation counter. HERFD spectra were measured by scanning the incident energy of X-rays at constant emission energy of the maximum of the Fe $K_{\beta 1,3}$ line (calibrated as 7059.5 eV with an iron foil). The overall energy resolution (monochromator and analyzers) estimated from the full width at half maximum of the elastic lines was found to be approximately 0.9 eV at an energy of 7060 eV. The samples were placed in Lucite holders with Kapton windows and measured at room temperature. The samples were monitored for radiation damage and the high flux of the beam decreased by Al absorbers (5–20%), until no damage was observed after 3 scans.

Data Reduction: The pre-edge and after-edge backgrounds of the conventional XANES spectra over a long-energy range (+400 eV) were analyzed with ATHENA.[44,45] Background reduction was achieved by using the Autobackup routine.[46] The high-resolution XANES scans were normalized to match the first and second resonances of the conventional XANES simulations, since the backgrounds cannot be determined because of the short-energy ranges. Edge positions were determined as the maximum of the first derivative.

Computational Methods: The atomic coordinates of the Fe^{III}-catecholate Sample **B** {compound [Fe^{III}(**L1**)(tcc)]} to build computer models (see details of the models in Results Section and Figure 1) were taken from the crystal structure CCDC-644244 of the six-coordinate compound[7] [Fe^{III}(**L3**)(tcc)(OH$_2$)] (with **L3**: 3,3-bis(1-ethyl-4-isopropylimidazol-2-yl)propionate). For the six-coordinate Sample **A**, the catechol ligand for the former compound was replaced by another ligand **L1** on the other side of the metal, and the structure was optimized by using a semiempirical model with Spartan Student Edition.[47] The coordinates of the 2-His-1-carboxylate model compound Sample **C** were taken from the crystal structure CCDC-626976.[8] The input files for FEFF were generated with CRYSTALFF.[48]

The "goodness" of the simulation was estimated by the position in energy of the spectral features and their relative intensity (see first derivative and difference spectra in the Supporting Information Figure 2).

XANES simulations were performed by using FEFF8.2.[15] The code uses the real-space multiple scattering theory and a self-consistent field calculation of the potentials, defined by using the muffin-tin prescription with 30% overlap. The atomic absorption μ was calculated by using the ground state potential, while for the excited state, the Hedin–Lundqvist exchange correlation potential was used. The conventional XANES simulations include the core-hole line broadening plus 0.5 eV that accounts for the experimental line broadening. The high-resolution XANES was simulated by suppressing the core-hole line broadening in the FEFF8 simulation.[49] The L densities of states without a core hole are obtained from the calculations. Simulations were performed on a single molecule, including all atoms of the coordinating ligands, which is usually enough for XANES and X-ray emission simulations in molecular

compounds and protein active sites[16,20,50] The cluster sizes and coordinates are as described in the Results Section.

Simulations with FDMNES[24] by using the finite difference method (FDM) to solve the Schrödinger equation were performed in order to assess the impact of the muffin-tin approximation in FEFF8. Because of the computational cost of the FDM method, only the best model for each sample were tested. The SCF calculation was performed up to the second coordination shell.[51] The transitions were broadened by using a Gaussian line to account for the broadening of the Si(111) monochromator (estimated at 1 eV) and Lorentzian lines with increasing broadening[51,52] (arctangent method) with a maximum of 6 eV at 10 eV above the edge to account for Plasmon effects. Simulations with and without core-hole broadening were performed.

The pre-edges were simulated by using the crystal field multiplet theory (CFM).[25,26] The code is basically the Cowan code,[53] further extended by B. T. Thole and F. M. F. de Groot. Crystal field values for well-defined symmetries are used.[34] For the case of Sample **B**, the symmetry was defined as O_h and for the five-coordinate ferric compound the O_h symmetry as well as models including distortion of the symmetry to C_{4v} were calculated. Sample **C** contains a chloride atom, which is expected to introduce an asymmetry in the crystal field not easy to predict without ab initio calculations. For this reason, it is not calculated in this paper.

Supporting Information (see footnote on the first page of this article): First derivatives of the experimental and most representative models for Sample **A** and **B**, difference spectra of the most representative models and the experimental high-resolution XANES, all simulated models with FEFF8, densities of states calculated with FDMNES, a typical $K_{\beta 1,3}$ emission spectrum and simulations of Sample **C** with chlorine replaced by fluor and the crystal field values of the CFM calculations are presented.

Acknowledgments

B. M. W. and R. J. M. K. G. thank the NRSCC (The Netherlands) for funding. Computing time was granted by the SARA computer facility in Amsterdam (The Netherlands) grant MP-06-124. The XANES experiments were carried out at SPring-8 under the proposal 2007A1292. This study was partially supported by a Grant-in-Aid for Scientific Research (B) (Grant No. 20350039) by MEXT, Japan. Sample **C** was kindly provided by Prof. William Tolman and Dr. Seth Friese (University of Minnesota, USA).

[1] L. Que Jr., *Nat. Struct. Biol.* **2000**, *7*, 182.
[2] E. I. Solomon, T. C. Brunold, M. I. Davis, J. N. Kemsley, S.-K. Lee, N. Lehnert, F. Neese, A. J. Skulan, Y.-S. Yang, J. Zhou, *Chem. Rev.* **2000**, *100*, 235.
[3] M. Costas, M. P. Mehn, M. P. Jensen, L. Que Jr., *Chem. Rev.* **2004**, *104*, 939.
[4] P. C. A. Bruijnincx, G. van Koten, R. J. M. Klein Gebbink, *Chem. Soc. Rev.* **2008**, *37*, 2716.
[5] T. D. H. Bugg, G. Lin, *Chem. Commun.* **2001**, 941.
[6] F. H. Vaillancourt, J. T. Bolin, L. D. Eltis, *Crit. Rev. Biochem. Mol. Biol.* **2006**, *41*, 241.
[7] P. C. A. Bruijnincx, M. Lutz, A. L. Spek, W. R. Hagen, B. M. Weckhuysen, G. Van Koten, R. J. M. Klein Gebbink, *J. Am. Chem. Soc.* **2007**, *129*, 2275.
[8] S. J. Friese, B. E. Kucera, L. Que, W. B. Tolman, *Inorg. Chem.* **2006**, *45*, 8003.
[9] A. L. Roe, D. J. Schneider, R. J. Mayer, J. W. Pyrz, J. Widom, L. Que Jr., *J. Am. Chem. Soc.* **1984**, *106*, 1676.
[10] C. R. Randall, L. Shu, Y. M. Chiou, K. S. Hagen, M. Ito, N. Kitajima, R. J. Lachicotte, Y. Zang, L. Que Jr., *Inorg. Chem.* **1995**, *34*, 1036.
[11] C. R. Randall, Y. Zang, A. E. True, L. Que Jr., J. M. Charnock, C. D. Garner, Y. Fujishima, C. J. Schofield, J. E. Baldwin, *Biochemistry* **1993**, *32*, 6664.
[12] T. E. Westre, P. Kennepohl, J. G. DeWitt, B. Hedman, K. O. Hodgson, E. I. Solomon, *J. Am. Chem. Soc.* **1997**, *119*, 6297.
[13] M. I. Davis, E. C. Wasinger, A. Decker, M. Y. M. Pau, F. H. Vaillancourt, J. T. Bolin, L. D. Eltis, B. Hedman, K. O. Hodgson, E. I. Solomon, *J. Am. Chem. Soc.* **2003**, *125*, 11214.
[14] J. G. Mesu, T. Visser, F. Soulimani, E. E. van Faassen, P. de Peinder, A. M. Beale, B. M. Weckhuysen, *Inorg. Chem.* **2006**, *45*, 1960.
[15] A. L. Ankudinov, B. Ravel, J. J. Rehr, S. D. Conradson, *Phys. Rev. B* **1998**, *58*, 7565.
[16] A. Mijovilovich, W. Meyer-Klaucke, *J. Synchrotron Radiat.* **2003**, *10*, 64.
[17] T. Burgdorf, S. Löscher, P. Liebisch, E. Van Der Linden, M. Galander, F. Lendzian, W. Meyer-Klaucke, S. P. J. Albracht, B. Friedrich, H. Dau, M. Haumann, *J. Am. Chem. Soc.* **2005**, *127*, 576.
[18] S. Löscher, I. Zebger, L. K. Andersen, P. Hildebrandt, W. Meyer-Klaucke, M. Haumann, *FEBS Lett.* **2005**, *579*, 4287.
[19] J. S. Magyar, T.-C. Weng, C. M. Stern, D. F. Dye, B. W. Rous, J. C. Payne, B. M. Bridgewater, A. Mijovilovich, G. Parkin, J. M. Zaleski, J. E. Penner-Hahn, H. A. Godwin, *J. Am. Chem. Soc.* **2005**, *127*, 9495.
[20] A. Mijovilovich, *Chem. Biodiversity* **2008**, *5*, 2131.
[21] H. Hayashi, Y. Udagawa, C.-C. Kao, *J. Electron. Spectrosc. Relat. Phenom.* **2004**, *137–140*, 277.
[22] W. M. Heijboer, P. Glatzel, K. R. Sawant, R. F. Lobo, U. Bergmann, R. A. Barrea, D. C. Koningsberger, B. M. Weckhuysen, F. M. F. de Groot, *J. Phys. Chem. B* **2004**, *108*, 10002.
[23] J. P. Rueff, L. Journel, P. E. Petit, F. Farges, *Phys. Rev. B* **2004**, *69*, 235107.
[24] Y. Joly, *J. Synchrotron Radiat.* **2003**, *10*, 58.
[25] F. M. F. de Groot, *J. Electron Spectrosc. Relat. Phenom.* **1994**, *67*, 529.
[26] F. M. F. de Groot, A. Kotani, *Core level Spectroscopies of Solids*, Taylor & Francis, New York, **2008**.
[27] H. Hayashi, S. Matsuo, T. Kurisaki, N. Kawamura, *X-ray Spectrom.* **2008**, *37*, 232.
[28] F. M. F. de Groot, *Coord. Chem. Rev.* **2005**, *249*, 31.
[29] W. Meyer-Klaucke, H. Winkler, V. Schuenemann, A. X. Trautwein, H.-F. Nolting, J. Haavik, *Eur. J. Biochem.* **1996**, *241*, 432.
[30] V. Schünemann, C. Meier, W. Meyer-Klaucke, H. Winkler, A. X. Trautwein, P. M. Knappskog, K. Toska, J. Haavik, *J. Biol. Inorg. Chem.* **1999**, *4*, 223.
[31] M. S. Chow, B. E. Eser, S. A. Wilson, K. O. Hodgson, B. Hedman, P. F. Fitzpatrick, E. I. Solomon, *J. Am. Chem. Soc.* **2009**, *131*, 7685.
[32] H. Modrow, S. Bucher, J. J. Rehr, A. L. Ankudinov, *Phys. Rev. B* **2003**, *67*, 351231.
[33] A. Pantelouris, H. Modrow, M. Pantelouris, J. Hormes, D. Reinen, *Chem. Phys.* **2004**, *300*, 13.
[34] F. M. F. de Groot, J. C. Fuggle, B. T. Thole, G. A. Sawatzky, *Phys. Rev. B* **1990**, *42*, 5459.
[35] F. M. F. De Groot, G. Vanko, P. Glatzel, *J. Phys. Condens. Matter* **2009**, *21*.
[36] H. Erlandsen, F. Fusetti, A. Martinez, E. Hough, T. Flatmark, R. C. Stevens, *Nat. Struct. Mol. Biol.* **1997**, *4*, 995.
[37] G. Smolentsev, A. V. Soldatov, E. C. Wasinger, E. I. Solomon, *Inorg. Chem.* **2004**, *43*, 1825.
[38] M. Benfatto, J. A. Solera, J. Garcia Ruiz, J. S. Chaboy, *Chem. Phys.* **2002**, *282*, 441.
[39] E. I. Solomon, A. Decker, N. Lehnert, *Proc. Natl. Acad. Sci. USA* **2003**, *100*, 3589.

[40] P. C. A. Bruijnincx, I. L. C. Buurmans, S. Gosiewska, M. A. H. Moelands, M. Lutz, A. L. Spek, G. Van Koten, R. J. M. Klein Gebbink, *Chem. Eur. J.* **2008**, *14*, 1228.
[41] H. Maruyama, M. Suzuki, N. Kawamura, M. Ito, E. Arakawa, J. Kokubun, K. Hirano, K. Horie, S. Uemura, K. Hagiwara, M. Mizumaki, S. Goto, H. Kitamura, K. Namikawa, T. Ishikawa, *J. Synchrotron Radiat.* **1999**, *6*, 1133.
[42] H. Hayashi, T. Azumi, A. Sato, Y. Udagawa, *J. Electron. Spectrosc. Relat. Phenom.* **2008**, *168*, 34.
[43] H. Hayashi, *Anal. Sci.* **2008**, *24*, 15.
[44] B. Ravel, M. Newville, *J. Synchrotron Radiat.* **2005**, *12*, 537.
[45] M. Newville, *J. Synchrotron Radiat.* **2001**, *8*, 322.
[46] M. Newville, P. Livins, Y. Yacoby, J. J. Rehr, E. A. Stern, *Phys. Rev. B* **1993**, *47*, 14126.
[47] www.Wavefun.com, **2004**.
[48] K. Provost, F. Champloy, A. Michalowicz, *J. Synchrotron Radiat.* **2001**, *8*, 1109.
[49] J. J. Rehr, *BIOXAS conference*, Soleil, France, **2007**.
[50] A. Mijovilovich, S. Hamman, F. Thomas, F. M. F. de Groot, B. M. Weckhuysen, *Phys. Chem. Chem. Phys.* **2011**, *13*, 5600.
[51] O. Bunau, Y. Joly, *J. Phys. Condens. Matter* **2009**, *21*, 345501.
[52] M. C. Feiters, G. A. Metselaar, B. B. Wentzel, R. J. M. Nolte, S. Nikitenko, D. C. Sherrington, Y. Joly, G. Y. Smolentsev, A. N. Kravtsova, A. V. Soldatov, *Ind. Eng. Chem. Res.* **2005**, *44*, 8631.
[53] R. D. Cowan, *The Theory of Atomic Structure and Spectra*, University of California Press, Berkeley, **1981**.

Received: October 7, 2011
Published Online: January 30, 2012

